A&A 517, A68 (2010)
DOI: 10.1051/0004-6361/201014723

Astronomy & Astrophysics

Generation of radiative knots in a randomly pulsed protostellar jet

II. X-ray emission

R. Bonito[1,2], S. Orlando[2], M. Miceli[1,2], J. Eislöffel[3], G. Peres[1,2], and F. Favata[4]

[1] Dip. Scienze Fisiche ed Astronomiche, Sez. Astronomia, Università di Palermo, P.zza del Parlamento 1, 90134 Palermo, Italy
e-mail: sbonito@astropa.unipa.it
[2] INAF – Osservatorio Astronomico di Palermo, P.zza del Parlamento 1, 90134 Palermo, Italy
[3] Thüringer Landessternwarte, Sternwarte 5, 07778 Tautenburg, Germany
[4] European Space Agency Community Coordination and Planning Office, 8–10 rue Mario Nikis, 75738 Paris Cedex 15, France

Received 2 April 2010 / Accepted 11 May 2010

ABSTRACT

Context. Protostellar jets are known to emit in a wide range of bands, from radio to IR to optical bands, and to date about ten jets that also emit X-rays have been detected, with a rate of discovery of about one per year.
Aims. We aim at investigating the mechanism leading to the X-ray emission detected in protostellar jets and in particular at constraining the physical parameters that describe the jet/ambient interaction by comparing our model predictions with observations available from the literature.
Methods. We perform 2D axisymmetric hydrodynamic simulations of the interaction between a supersonic jet and the ambient medium. The jet is described as a train of plasma blobs randomly ejected by the stellar source along the jet axis. We explore the parameter space by varying the ejection rate, the initial Mach number of the jet, and the initial density contrast between the ambient medium and the jet. We synthesize the X-ray emission from the model as it would be observed with the current X-ray telescopes.
Results. The mutual interactions among the ejected blobs themselves and of the blobs with the ambient medium lead to complex X-ray-emitting structures within the jet. The X-ray sources consist of several components: irregular chains of knots, isolated knots with measurable proper motion, apparently stationary knots, and reverse shocks. The predicted X-ray luminosity strongly depends on the ejection rate and on the initial density contrast between the ambient medium and the jet, with a lesser dependence on the jet Mach number.
Conclusions. Our model represents the first attempt to describe the X-ray properties of all X-ray-emitting protostellar jets discovered so far. The comparison between our model predictions and the observations can provide a useful diagnostic tool, which is necessary for a proper interpretation of the observations. We specifically suggest that the observable quantities derived from the spectral analysis of X-ray observations can be used to constrain the ejection rate, a parameter explored in our model that is not measurable by current observations in all wavelength bands.

Key words. hydrodynamics – Herbig-Haro objects – ISM: jets and outflows – X-rays: ISM

1. Introduction

In the first decade of this century, high-energy emission from protostellar jets (originally suggested by Pravdo & Marshall 1981) has been discovered, taking advantage of both the high spatial resolution of Chandra and the high effective area of *XMM-Newton*. To date, about ten X-ray-emitting Herbig-Haro (HH) objects are known, whose main emission properties are reviewed in Table 1 (see also Bonito et al. 2007).

The X-ray sources detected in HH jets are characterized by different morphologies, luminosities, and locations within the jet. In some cases, the X-ray-emitting region is located at the base of the (optical) jet, near the protostar from which the jet originates. This is the case, for instance, for the low-mass (LM) HH 154 and DG Tau jets, both in Taurus (see Bally et al. 2003; Güdel et al. 2005). In other cases, the X-ray source is located farther away from the protostar as, for example, for the high-mass (HM) HH 80/81 jet. Concerning the morphology, some of the X-ray sources cannot be resolved by current instruments (and appear point-like), some others appear to be elongated. In one case (HH 154) a knotty X-ray source is found (resembling the knotty morphology commonly observed in the optical emission from HH jets), which consists of an elongated tail with a measurable proper motion away from the stellar source and an apparently stationary point-like source (Favata et al. 2006).

Current models, aimed at explaining the origin of X-ray emission from protostellar jets, considered a continuous supersonic jet propagating through a homogeneous interstellar medium (Bonito et al. 2004, 2007). These models succeeded in predicting X-ray sources associated with jets with luminosity and proper motion in good agreement with the observations. They failed, however, in reproducing the complex knotty morphology of the X-ray source detected in HH 154 (Favata et al. 2006).

In a previous paper (Bonito et al. 2010; hereafter Paper I), we proposed an improvement to these models by considering the scenario based on a pulsed jet, i.e. a jet characterized by an ejection velocity varying randomly in time, and interacting with an initially homogeneous ambient medium. The aim was to investigate the origin of the irregular knotty structure observed in protostellar jets in different wavelength bands and the complex

Table 1. Physical properties observed in X-ray-emitting HH jets.

object	t_{exp} [ks]	cnts	L_X [10^{29} erg s^{-1}]	T_X [10^6 K]	L_j [arcsec]	z_X [AU]	D [pc]	LM/HM	Reference
HH 2	21.4	11	5.2	1	2	56 000[c]	480	LM	Pravdo et al. (2001)
HH 154	97	63	3	4	5	70–140	140	LM	Favata et al. (2006)[d]
HH 80/81	37.3	46/63	450/430	1.5	–	515 000	1700	HM	Pravdo et al. (2004)
HH 168	78	–	30	6.5	–	–	730	HM	Pravdo et al. (2009)
HH 210	838	31	10	0.8	–	37 000[c]	450	HM	Grosso et al. (2006)
HH 540	795.8	≈200	0.4	6.6	–	<90	450	LM	Kastner et al. (2005)[a]
HH 216	78	8	10	–	4	–	2000	–	Linsky et al. (2007)
DG Tau	90	18; 9[b]	0.12	3.4	5	30	140	LM	Güdel et al. (2008)
Z CMa	39.6	20	>2.6	2.3	–	>2000	1050	HM	Stelzer et al. (2009)
TKH 8	89.2	28	20	35.4	–	450–900	450	LM	Tsujimoto et al. (2004)[e]

Notes. t_{exp} is the exposure time of the observations (or the total exposure time adding together several observations, as in the case of DG Tau); cnts are the collected photons; L_X is the X-ray luminosity roughly in the [0.3−10] keV band; T_X is the best fit temperature; L_j is the linear size of the X-ray source; z_X is the distance of the X-ray source from the central protostar; D is the distance of the HH object; LM/HM indicates the low-mass or high-mass young stellar object from which the jet originates.
[(a)] Improved estimates of L_X and T_X from Joel Kastner and Ettore Flaccomio, private communication.
[(b)] The first value is associated with the South-Western jet and the second with the North-Eastern jet in DG Tau.
[(c)] Values derived from SIMBAD.
[(d)] See also Bally et al. (2003).
[(e)] See also Tsuboi et al. (2001).

interactions occurring among blobs of plasma ejected from the stellar source. Our analysis showed that the mutual interactions of blobs ejected at different epochs and with different speed naturally reproduce the irregular pattern of knots observed along the jet axis in many HH objects and lead to a variety of plasma components which cannot be described by models of a jet ejected with a sinusoidal variable velocity (e.g. Raga et al. 2007).

Here we further explore the model of a randomly ejected pulsed jet presented in Paper I with the aim to investigate the properties of its X-ray emission and how these properties may depend on the physical conditions in which the jet evolves. Indeed, X-ray emission from jets is observed in HH objects at different evolutionary stages and with different masses: for instance, HH 154 originates from a LM binary system of class 0 and class I sources; DG Tau is a more evolved LM classical T Tauri star; HH 80/81 originates from an HM pre-main-sequence star. Given the wide range of conditions in which X-ray emission from jets originates, it is important to address the following issues: where and when is the X-ray emission expected to arise from HH jets? How common is the high-energy emission from HH jets?

The paper is organized as follows: in Sect. 2 we present our model, in Sect. 3 we show our results concerning the morphology and luminosity in the X-ray band, in Sect. 4 we discuss our results, and in Sect. 5 we draw our conclusions.

2. The model

We model the evolution of a protostellar jet ejected with a supersonic random speed and ramming into an initially homogeneous ambient medium. A detailed description of our model can be found in Paper I, to which the reader is referred for more details. We briefly recall that we performed 2D hydrodynamic simulations of the interaction between the jet and the ambient medium in a cylindrical coordinate system (r, z) by solving the equations of conservations of mass, momentum, and energy, with the FLASH code (Fryxell et al. 2000). The model takes into account the radiative losses from optically thin plasma and the thermal conduction in both the Spitzer (Spitzer 1962) and saturated (Cowie & McKee 1977) regimes.

Axisymmetric boundary conditions are imposed along the jet axis (consistent with the adopted symmetry), inflow boundary conditions at the base for $r < r_j$, where r is the radial distance from the jet axis in cylindrical coordinates and $r_j \approx 30$ AU is the jet radius, and outflow boundary conditions elsewhere (see also Paper I). The spatial resolution achieved in our simulations is about 8 AU, i.e. about eight times the resolution of Chandra/ACIS-I observations at a distance of ≈150 pc (i.e. roughly the distance of the closest star-forming region; SFR).

The time covered by our simulations ranges between 100 years and 400 years, depending on the initial setup of the model. The jet is described as a train of blobs, each lasting for half a year, with an ejection rate corresponding to a time interval between the ejection of two consecutive blobs $\Delta t = 0.5, 2, 8$ yr. The initial setup is derived from the analysis of the optical and X-ray data and from the results of previous models (Bonito et al. 2007). Each blob is ejected with a random velocity directed along the jet axis (the z-axis), sampled from an exponential distribution, and with a maximum velocity v_j, corresponding to the initial Mach number $M = v_j/c_s$, where c_s is the sound speed (see Paper I for more details).

We explore both the initial light jet scenario (a jet initially less dense than the unperturbed ambient medium; hereafter LJ runs), and the initial heavy jet scenario (a jet initially denser than the ambient medium; hereafter HJ runs). Note that the concept of a light and a heavy jet is limited to the initial conditions of our simulations. Indeed, as already discussed in Paper I, the density contrast between the ambient medium and the blob can vary during the jet/ambient evolution, the density of the medium varying by several orders of magnitude after the first high-speed blob has perturbed the whole computational domain (see Fig. 3 of Paper I). In other words, the ejected blobs can be denser or less dense than the medium in which they propagate in each of the simulations considered here. Table 2 summarizes the physical parameters characterizing the simulations. In all models we assume $r_j \approx 30$ AU as the initial jet radius and derive $T_a = 10^3$ K

Table 2. Summary of the initial physical parameters characterizing the simulations (see text for details).

Model	Δt [yr]	ν	M	v_j [km s^{-1}]	T_j [K]	n_a [cm^{-3}]
LJ0.5-M1000	0.5	10	1000	10–4680	10^4	5000
LJ2-M1000	2	10	1000	10–4680	10^4	5000
LJ8-M1000	8	10	1000	10–4680	10^4	5000
LJ2-M100	2	10	100	10–470	10^4	5000
LJ2-M300	2	10	300	10–1400	10^4	5000
LJ2-M500	2	10	500	10–2340	10^4	5000
HJ2-M300	2	0.1	300	10–1400	10^2	50
HJ2-M500	2	0.1	500	10–2340	10^2	50
HJ2-M1000	2	0.1	1000	10–4680	10^2	50

Notes. Δt is the time interval between two consecutive blobs, ν is the ambient-to-jet density contrast, M is the Mach number of the first blob, v_j is the velocity of each ejected blob (here we indicate the range of values randomly generated by our model), T_j is the initial jet temperature, and n_a is the ambient density.

as the initial ambient temperature, assuming initial pressure balance between the jet and the ambient medium.

3. Results

The dynamics and energetics of the randomly ejected pulsed jet have been extensively described in Paper I. Here we focus on the analysis of the X-ray emission predicted to arise from the pulsed jet. The X-ray emission is synthesized from the model results by adopting the methodology described in Bonito et al. (2007) that allows us to derive images and spectra of the X-ray sources associated with the jets. In short, we first recover the 3D spatial distributions of density and temperature by rotating the corresponding 2D distributions around the symmetry z axis ($r = 0$). Then we integrate along the line of sight[1] with the assumption of an optically thin plasma, and derive the emission measure distribution as a function of the temperature, EM(T)[2]. Using available spectral emission codes and taking into account both the instrumental response and the interstellar absorption, we derive the X-ray spectra, the morphology, and the evolution of the X-ray luminosity, L_X, to be compared directly to the parameters derived from the observations.

3.1. Morphology of X-ray jets

We investigate the morphology of the X-ray sources associated with jets by simulating observations with Chandra/ACIS-I, which is currently the X-ray instrument with the highest spatial resolution. As an example, Fig. 1 shows the X-ray emission in the [0.3−10] keV band (left panel) and the corresponding mass density distribution (right panel) for run LJ0.5-M1000, assuming a distance of 150 pc and an absorption column density $N_H = 1.4 \times 10^{22}$ cm^{-2}, as derived for the HH 154 jet. In general the morphology of the source is quite complex, showing several X-ray-emitting plasma components: knots resulting from the interaction among different blobs[3] of plasma ejected from the stellar source (for instance see left panel in Fig. 1),

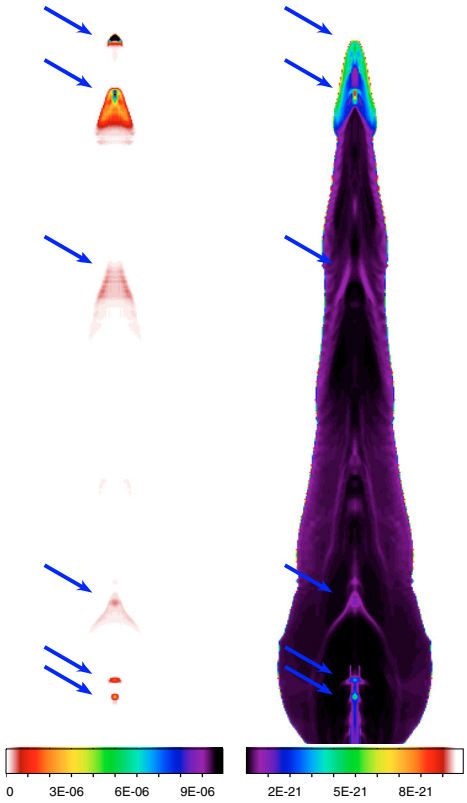

Fig. 1. X-ray image of the jet synthesized from the pulsed jet model in the [0.3−10] keV band (*left panel*) and corresponding mass density distribution (*right panel*) 31 years after the beginning of the simulation in run LJ0.5-M1000. The blue arrows superimposed on each panel mark the same positions in the X-ray map and mass density distribution. The size of the jet is about 4600 AU, corresponding to ≈30″ at 150 pc.

reverse shocks interacting with outgoing knots, stationary knots, oblique structures.

The most striking feature in Fig. 1 (left panel) is the irregular pattern of knots aligned along the jet axis, which are possibly interacting with each other, analogous to the well-known optical knotty structure observed within HH jets. This complex chain of X-ray knots originates in the interaction of different ejected blobs with each other and with the inhomogeneous medium into which they propagate. Indeed, as explained in Paper I, the initially homogeneous ambient medium becomes quickly inhomogeneous because the blobs ejected with different speeds and at different epochs perturb the medium and strong variations of the pre-shock conditions occur (see also Fig. 3 in Paper I). Chains of knots are particularly evident for high ejection rates; for instance, we found up to six knots for $\Delta t = 0.5$ yr (see left panel in Fig. 1). The X-ray sources along the jet axis are associated with strong shocks visible in the density distribution (see right panel of Fig. 1). In general, the brightest X-ray knots occur at the base of the jet and are due to the ejection of single blobs of plasma with high speed into the ambient medium. X-ray emission from isolated knots created by a single high-speed ejected blob is common to all the runs discussed here.

In principle it is possible to derive the proper motion of modeled X-ray knots and compare it to the measured or expected proper motion from observed X-ray sources in protostellar jets. Our simulations have shown that the knot speed ranges between 300 and 3000 km s^{-1} (i.e. between 0.4″/yr and 4″/yr at 150 pc). As an example, Fig. 2 shows the evolution of the

[1] Assumed to be perpendicular to the jet axis.
[2] See Bonito et al. (2007) for definitions and details on the EM.
[3] As discussed in Paper I, we use the term "blob" to indicate the ejected clump of plasma and "knot" to indicate the observable structure formed along the jet.

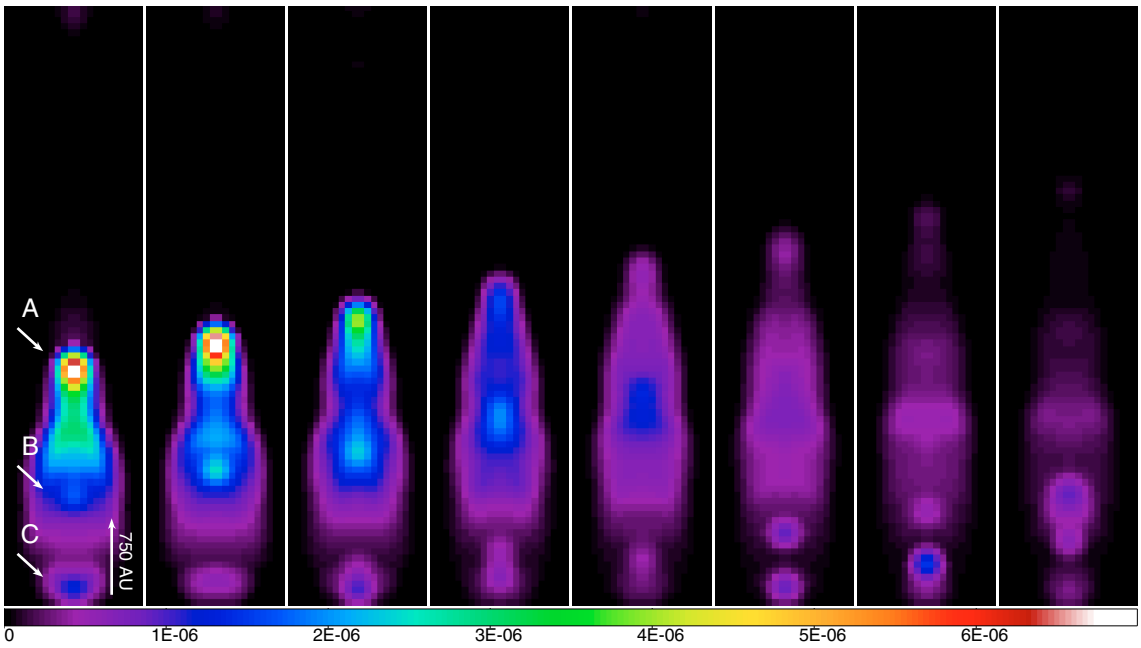

Fig. 2. Evolution of the X-ray emission as it would be observed with Chandra/ACIS-I in run LJ0.5-M1000. The head of the jet is outside the spatial domain. Two consecutive panels are separated by a time interval of 0.5 years, the first panel corresponding to 44 years since the beginning of the jet/ambient interaction. The spatial scales are shown in the first frame as well as the three main sources highlighted by the arrows: knots A, B, and C.

X-ray emission for run LJ0.5-M1000; the proper motion of X-ray-emitting knots A, B, and C is measurable in a few years. The knots speed deduced from these measurements ranges between about 300 km s^{-1} for the C knot at the base of the jet, and 2000 km s^{-1} (i.e. 3″/yr at 150 pc) for the bright A knot. It is remarkable that the faint and slow C knot at the base of the jet is persistent throughout the evolution of the jet shown in Fig. 2, due to continuous fueling by subsequent ejected blobs; on the other hand the brightest source (A knot), which shows the highest proper motion, cools down and its X-ray luminosity drops by about one order of magnitude after about two years. Unfortunately the only X-ray-emitting jet for which it was as yet possible to measure the proper motion of the X-ray source (≈500 km s^{-1}) is HH 154 (Favata et al. 2006). For this case, our model predictions agree well with the observations, because the characteristic values of the average knot speeds derived from our model are consistent with the value of a few hundreds km/s (see Fig. 10 of Paper I). Nonetheless, our analysis suggests that in general a measurable proper motion of X-ray knots is expected and our predictions can be challenged in future observations (see, however, possible misinterpretations of observations discussed in Sect. 4.2).

Additional contributions to X-ray emission may come from a variety of complex plasma structures formed within the jet due to interactions among supersonic blobs, shocks, and the cocoon enveloping the jet. In particular, oblique structures can form at the cocoon (see also Paper I), as well as reverse shocks that travel in the opposite direction of the ejected blobs (i.e. toward the stellar source) and that possibly interact with them. Under certain circumstances, shocks formed within the jet may show no proper motion on time-scales of a few years. As an example, Fig. 3 shows an almost stationary X-ray source in run LJ2-M1000 over a time-scale of about 5 years caused by the interaction of a reverse shock with outgoing plasma blobs.

The position of the X-ray sources can be compared to that of expected optical knots by deriving density maps of plasma with

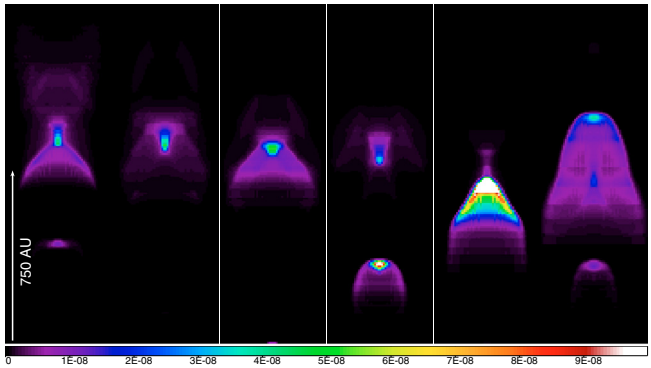

Fig. 3. Zoom of the X-ray emission at the base of the jet for run LJ2-M1000 over a time baseline of about 5 years. The spatial scale is shown in the first frame (750 AU correspond to 5″ at 150 pc).

the temperature ranging between (5×10^3–10^5) K, which is a proxy of optical emission (see Paper I). As an example, Fig. 4 shows the evolution of both expected optical knots and X-ray sources in run HJ2-M300. The X-ray sources are in general not co-spatial with optical knots. Indeed, the figure shows a weak X-ray source located at the base of the chain of optical knots, showing a stratification of the X-ray and optical emission.

3.2. X-ray light curves

We derived the X-ray luminosity, L_X, and its evolution for all runs listed in Table 2. Our model predicts significant X-ray emission in the light jet scenario (LJ runs in Table 2) and very faint or no X-ray emission in the heavy jet scenario (HJ runs in Table 2; compare the different scales in Fig. 1 and Fig. 4). In this section, we therefore focus on LJ runs that predict X-ray emission detectable with current X-ray observatories.

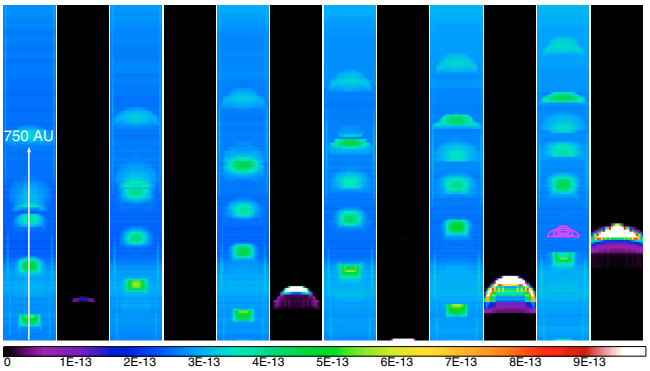

Fig. 4. Evolution of both expected optical knots (odd panels) and X-ray emission (even panels) in run HJ2-M300. The contours of the brightest regions of the X-ray source in the last panel are superimposed on the corresponding optical image. The spatial scale is shown in the *first panel*.

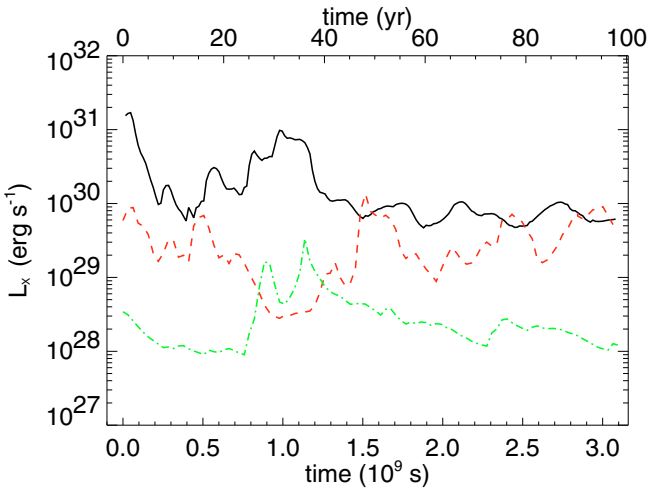

Fig. 5. Evolution of the X-ray luminosity derived from runs LJ0.5-M1000 (solid line in black), LJ2-M1000 (dashed line in red), and LJ8-M1000 (dashed-dotted line in green). Time =0 corresponds to 2.5 years, 10 years, and 40 years from the beginning of the simulation for run LJ0.5-M1000, LJ2-M1000, and LJ8-M1000, respectively.

In our simulations, the maximum value of L_X is reached when the first blob (characterized by the highest allowed velocity) is ejected in the unperturbed ambient medium. Because this high-speed blob and its interactions with subsequent ones cause the formation of very bright sources that are clearly due to the initial transient configuration, we removed the contribution to L_X that stemmed from the first three ejected blobs[4]. Figure 5 shows L_X as a function of time for runs LJ0.5-M1000 (solid line in black), LJ2-M1000 (dashed line in red), and LJ8-M1000 (dashed-dotted line in green), after the transient phase has been removed. Typical values of L_X range between 10^{28} erg s^{-1} and a few 10^{31} erg s^{-1}, which agrees well with almost all observations of X-ray-emitting HH jets.

Figure 5 shows that L_X depends on the velocity of the ejected blobs and on the ejection rate. In particular, the X-ray luminosity decreases by three orders of magnitude from $\Delta t = 0.5$ yr to $\Delta t = 8$ yr, whereas it can vary by a factor 10 in each simulation depending on the velocity variations of the ejected blobs. This small variation of the X-ray luminosity with the velocity is also found by comparing the values of L_X derived from simulations with the same ejection rate ($\Delta t = 2$) and different Mach numbers, $M = 100, 300, 500$ (runs LJ2-M100, LJ2-M300, and LJ2-M500 in Table 2). We conclude therefore that the critical parameter in determining the X-ray luminosity of a protostellar jet is the ejection rate of plasma blobs rather than their velocities: the higher the ejection rate, the brighter the X-ray source associated with the jet. Indeed, the X-ray emission originates mainly in multiple interactions among knots and blobs, which increase for higher ejection rates.

[4] For this reason the epoch time = 0 in Fig. 5 corresponds to 2.5 years, 10 years, and 40 years from the beginning of the simulation for run LJ0.5-M1000, LJ2-M1000, and LJ8-M1000, respectively.

4. Discussion

4.1. Visibility of X-ray emission from HH jets

Although hundreds of HH jets have been revealed in several bands[5] (from radio to IR, to optical wavelength bands) up to now, only ten HH objects are known to emit also in X-rays (Table 1; see also Bonito et al. 2007). The small fraction of jets visible in the X-ray band poses a problem because in principle all high speed jets should emit X-rays. Of course, it is possible that X-ray emission from HH jets can be observed only under favorite conditions. Indeed, X-ray-emitting jets have to be sufficiently luminous to be detected in far away SFRs. Chandra observations of HH 154, the most luminous X-ray-emitting HH jet detected in the nearest SFR, collected about 60 counts in 100 ks (Favata et al. 2006); and even worse statistics have been obtained for the less luminous X-ray jet revealed in the same SFR and associated with DG Tau (Güdel et al. 2008). These sources, therefore, are intrinsically faint, and analogous ones located at larger distances cannot be detected with current instruments. It is therefore not surprising that X-ray jets located farther away are very bright, as in the case of the most luminous X-ray-emitting HH object revealed up to now, HH 80/81 (Pravdo et al. 2004).

Our simulations have shown that the necessary conditions for detectable X-ray emission from a randomly pulsed jet are both a high ejection rate and a high density of the medium into which subsequent plasma blobs are ejected. As an example, in a light jet (i.e. the scenario leading to detectable X-ray emission) the X-ray emission produced by a single blob interacting with the surrounding medium can be rather faint, or not present at all, if the ambient-to-blob density contrast is low, unless the blob propagates with very high speed (>2000 km s^{-1}).

As for the optical emission, the train of blobs forming the jet builds up a cocoon enveloping the jet and the subsequently ejected blobs. In the light jet scenario, this cocoon is characterized by high mass-density and is the dominant component in the optical emission, thus any contribution from internal knots in this band is negligible. Conversely, the density of the cocoon is much lower in the heavy jet scenario than that of the ejected blobs and the main contribution to the optical emission comes from the dense knots formed within the jet (see Fig. 4). Our model therefore predicts that light jets can lead to observable X-ray emission, but do not produce observable optical knots, whereas heavy jets reproduce the chains of optical knots commonly observed in almost all the known protostellar jets, but do not lead to detectable X-ray emission.

The different characteristics of the light and heavy jets that we discussed stem from the traveling knots, which are decelerated by a factor of about three by the surrounding dense medium

[5] A catalogue of HH objects has been prepared by B. Reipurth and can be found in http://casa.colorado.edu/hhcat/.

in the light jets. In the heavy jets the knots are only slightly decelerated by the medium into which they propagate (Bonito et al. 2007). New ejected blobs therefore travel into a medium constituted by strongly decelerated blobs in light jets and by several high-speed blobs in heavy jets. The average relative velocity between two consecutive blobs therefore is expected to be higher in light jets than in heavy jets, leading in general to X-ray emission in the former and to optical emission in the latter as a consequence of blob collisions.

At variance with our model predictions, however, X-ray-emitting jets also show a knotty morphology in the optical band. A possible way to reconcile model predictions and observations (i.e. reproducing both X-ray and optical knots in a single run) is to consider the generation of knots into a medium partly constituted by high-speed blobs and partly by strongly decelerated blobs. In this case the relative velocity between two consecutive blobs is expected to be low on average in the part with high-speed blobs, leading to optical emission, and high in the part with decelerated blobs, leading to X-ray emission. This scenario may be reproduced by considering an ejection direction varying in time. If the blob is ejected into a co-moving medium filled by previously ejected high-speed blobs, the average relative velocities between two blobs is expected to be low, leading to optical knots. Otherwise, if the blob is ejected into an almost stationary medium (because of the strong deceleration of previously ejected blobs), the average relative velocities between blobs are high and the knots resulting from the blob interactions may be observed in the X-rays. The above scenario is supported by the evidence that the location of the X-ray source in HH 154 is not completely aligned with the optical jet, as shown in Fig. 13 of Bonito et al. (2008).

4.2. Interpretation of X-ray observations of HH jets

As already discussed above, X-ray-emitting jets are faint sources and only limited spectral and morphological analyses can be performed with the instruments in operation at present. The modeling of the X-ray emission from protostellar jets can therefore be an important tool in the interpretation of observations and may provide crucial information to unveil the nature of the X-ray emission.

Our model has shown that a specific feature of a randomly pulsed jet is the mutual interaction between plasma blobs that leads to irregular patterns of knots aligned along the jet axis, which are possibly interacting with each other. The knots preferentially emit in the X-ray band in light jets and in the optical band in heavy jets. However, although chains of optical knots are commonly observed in almost all HH jets, current X-ray observations do not allow to reveal the predicted knotty structure of X-ray jets due to limited statistics. The only jet for which it was possible to analyze the morphology of the X-ray source is HH 154, thanks to its proximity and brightness (Favata et al. 2006). In this case, a knotty structure in the X-ray band has been revealed, which agrees with our model predictions and is somewhat correlated to the observed knotty structure in the optical band (Bonito et al. 2008). This feature is probably common to all X-ray-emitting jets, but is difficult to observe because of limited statistics.

For instance, a knotty structure of the X-ray jet may be hidden in the current observations of DG Tau. Güdel et al. (2008) analyzed the X-ray source associated with this jet and needed to co-add several different observations collected over a time-scale of three years to improve the statistics. Consequently, any information on the spatial structure of the X-ray source has been averaged over three years, making it impossible to reveal its true morphology. In the co-added image, these authors noted an elongated X-ray source with a spatial scale of about 5″ that originates from the central protostar. However, the observations of DG Tau cannot exclude that the X-ray source is constituted by several outgoing knots. Figure 6 shows the evolution of the X-ray emission for run LJ0.5-M1000 at the same resolution as the Chandra/ACIS-I instrument (panels 1−8): once several different frames separated in time by a few years have been summed (see last two panels in the figure), the knotty morphology clearly evident in the single frames cannot be recovered in the summed image that shows an almost continuous X-ray-emitting structure along the jet axis, with spatial scales of about 5″, similar to that derived by Güdel et al. (2008). Indeed, even if the proper motion of the single X-ray knot may be negligible in a few years (as explained by Güdel et al. 2008), it is important to take into account the fast variability of the structures within the jet and the radiative time-scales, which determine the lifetime of the knots. A knot can disappear over this time-scale and new ejected blobs can form new observable knots.

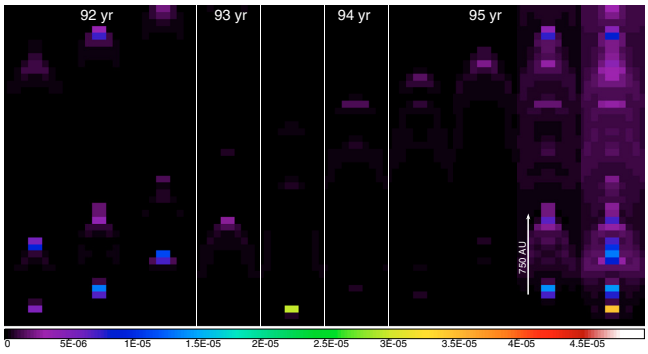

Fig. 6. Evolution of the X-ray emission in the LJ0.5-M1000 run. *First to eighth panels*: two consecutive panels are separated by a time interval of 0.5 years, the first panel corresponding to 91.5 years since the beginning of the jet/ambient interaction and the last to 95 years. The *ninth panel* shows the 92 years frame, 93 years frame, 94 years frame, and 95 years frame added together (the spatial scale is also shown: 750 AU correspond to 5″ at 150 pc). The *tenth panel* shows the sum of the first to eighth frames.

Another important contribution to the X-ray emission from HH jets comes from reverse shocks traveling in the opposite direction of ejected blobs, which possibly interact with them (see Sect. 3.1). These features are in general less frequent and shorter-lived (lasting for less than about 5 years) than the X-ray knots previously discussed, but are not negligible. They predict X-ray sources within the jet with no appreciable proper motion and may for instance explain the apparently stationary X-ray source detected at the base of the optical jet HH 154 over a time baseline of 4 years (Favata et al. 2006; Bonito et al. 2008). An example of this feature is an X-ray-emitting source roughly at the same position due to a reverse shock powered by subsequent interactions with outgoing plasma blobs shown in Fig. 3. A series of observations of this source on a baseline of 4 years may erroneously interpret the multiple interaction of the shock with subsequent blobs as a stationary X-ray source located at the base of the jet. This example shows how the comparison between model predictions and observations may be a useful tool in the data interpretation.

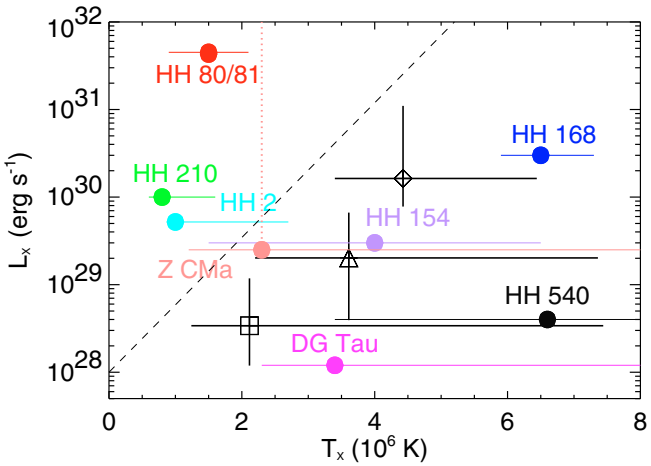

Fig. 7. X-ray luminosity as a function of best-fit temperature for the three cases of ejection rate considered: Δt = 0.5 (diamond), 2 (triangle), and 8 (square) yr. The dots superimposed to the figure mark the values derived from the observations of all known X-ray-emitting HH jets. The error bars of observed values are given if reported in the literature. The X-ray luminosity of Z CMa is not well constrained and only a lower limit is reported (pink dotted vertical line).

4.3. Comparison between model predictions and observations of X-ray-emitting jets

X-ray observations of HH jets allow us to derive the luminosity and best-fit temperature of the X-ray sources associated with the jets (see Table 1). The comparison between these observed values and those derived from our model may contribute useful information about the properties of X-ray emission from protostellar jets. Figure 7 shows the X-ray luminosity, L_X, versus the best-fit temperature, T_X, as a function of the ejection rate, derived from the analysis of spectra synthesized from runs LJ0.5-M1000, LJ2-M1000, and LJ8-M1000 (assuming high statistics, 10^4 total counts; see details in Bonito et al. 2007). The symbols and the bars in the figure represent the median values of L_X and T_X and the 10th and 90th percentiles ranges, respectively. Each simulation predicts a wide range of variation for both the L_X and the T_X, which is possibly related to the complex knotty morphology and fast variability (a few years) of X-ray jets. As expected, the most energetic case considered (Δt = 0.5 yr) leads to the highest luminosity and temperature: the higher Δt, the lower L_X and T_X.

Figure 7 also shows the X-ray luminosity and temperature derived from X-ray observations for all cases where some indication of L_X and T_X has been reported in the literature (see Table 1). Note that error bars are given in Fig. 7 if reported in the literature. The dashed line superimposed to the figure is arbitrary and separates HH objects characterized by X-ray emission close to the base of the jet (within ≈2000 AU from the stellar source; to the right) from HH objects showing X-ray emission at large distances (several thousands of AU) from the young stellar object (YSO) from which the jet originates (to the left; see Table 1). Figure 7 shows that HH jets with X-ray emission at the base of the jet have luminosities and temperatures that nicely agree with our model predictions. In particular, the HH 154 jet is well described by a pulsed jet with Δt = 2 yr. Remarkably, this result agrees well with the independent estimate of morphological evolution time-scale of the optical knots discussed by Bonito et al. (2008). DG Tau is the weakest X-ray-emitting jet (see Table 1) and is consistent with a jet with low ejection rate (i.e. the case that shows the lowest luminosities). Conversely, HH jets with X-ray emission at large distances from the YSO (namely HH 80/81, HH 210, and HH 2) are characterized by very low values of temperature (≈1 MK) and high luminosities (>10^{29} erg s^{-1}) and do not match with our model results. The jet associated with Z CMa appears to be intermediate to the two cases discussed above, in fact the distance of the X-ray source from the YSO is >2000 AU. In the framework of our model, we can interpret the X-ray knots located farther away from the YSO as due to strongly decelerated (and radiatively cooled) plasma blobs at low temperatures. In general, our model provides the first attempt to describe the characteristics of almost all the X-ray-emitting HH jets detected so far.

4.4. Location of X-ray sources within the jet

Another important parameter that allows us to compare model predictions with observations is the position of X-ray sources within the jet. In order to infer the position that is the most likely to be detected within the jet, we integrated the spatial distribution of X-ray emission derived from the model both along the radial direction and in time. This analysis requires that the computational domain has been already fully perturbed by the first high-speed blob (ejected with the maximum initial velocity) to avoid the initial transient phase. The time interval of the integration therefore varies for the different ejection rates considered: from 40 to 100 years for Δt = 0.5 yr, from ≈90 years to ≈140 years for LJ2-M1000, and from 220 to 400 years for Δt = 8 yr, the head of the jet traveling outside the domain after ≈40 years in the former case and ≈220 years in the latter case. Figure 8 shows the normalized count rate integrated along the jet axis and in time for the LJ0.5-M1000 (solid line in black), the LJ2-M1000 (dashed line in red), and the LJ8-M1000 run (dashed-dotted line in green). Most of the emission is located at the base of the jet, within about 1500 AU, with a first bump within about 200 AU from the YSO. The position of observed X-ray sources associated with HH jets is superimposed on the figure for the cases that show emission close to the base of the jet (i.e. HH jets to the right of the dashed line in Fig. 7). From the nearest to the farthest from the protostar: DG Tau (in magenta), HH 154 (in violet), HH 540 (in green), TKH 8 (in cyan), and Z CMa (in red).

The X-ray emission is highest (and, therefore, more easily detectable) at the base of the jet. Indeed, the interactions among blobs and, possibly, among knots involve higher energies close to the jet base than at longer distances and the outgoing knots progressively fade as they propagate away from the stellar source due to radiative cooling. We note that the position of observed X-ray-emitting sources associated with HH jets seems to be related to the mass of the central object from which the jet originates. In particular, almost all LM objects show emission localized preferentially at the base of the jet (see Fig. 8), with the exception of HH 2. On the contrary, the X-ray sources detected in the HM jets HH 80/81 and HH 210 are located at distances >5 × 10^4 AU from stellar source (not reported in the figure).

4.5. Predictions about future X-ray observations of HH 154

Among the known X-ray-emitting jets, HH 154 is the only one that allows us to challenge the predictions of our model because of its proximity and brightness. It is more specifically the only object for which it was possible to analyze the morphology and time variability in the X-ray band to date (Favata et al. 2006). The HH 154 X-ray source has been detected as an almost point-like source in 2001 (Bally et al. 2003) and as a knotty source,

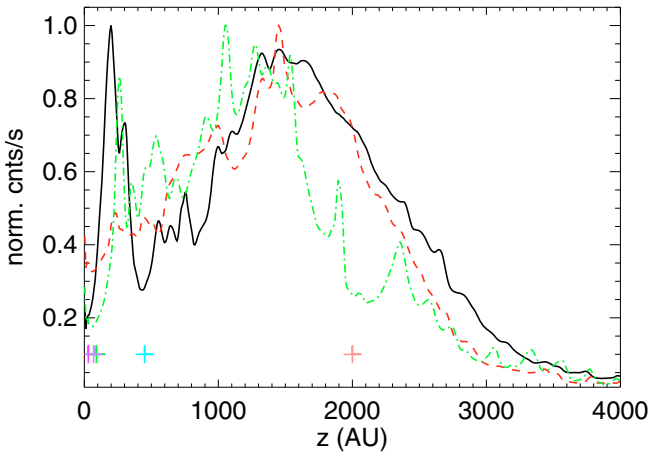

Fig. 8. Normalized count rate in the band [0.3−10] keV integrated over the radial direction and in time along the axis of the jet within 4000 AU for the LJ0.5-M1000 (solid line in black), the LJ2-M1000 (dashed line in red), and the LJ8-M1000 (dashed-dotted line in green) run after the computational domain has been fully perturbed by the first blob ejected (see text for details). The crosses superimposed indicate the position of observed X-ray sources associated with HH jets for those cases that show emission close to the base of the jet. From the nearest to the farthest from the stellar source: DG Tau (in magenta), HH 154 (in violet), HH 540 (in green), TKH 8 (in cyan), and Z CMa (in red).

consisting of a stationary (over a time baseline of 4 years) and an elongated source (showing a proper motion of ≈500 km s^{-1}) in 2005 (Favata et al. 2006). New future observations of this object promise therefore to add important pieces of information to shed light on the nature of the X-ray emission from jets. Here we use the results of our pulsed jet model to interpret future observations of HH 154.

- **Stationary source.** As discussed in Sect. 4.2, a pulsed jet with a random ejection speed can lead to the same configuration (i.e. an apparent stationary source) if the X-ray emission detected at different epochs arises from different knots that brighten roughly at the same position. However, the probability to see an almost stationary source is lower than the probability to see single moving knots according to our model, although it is not completely rejectable. Here we therefore cannot exclude alternative scenarios to that of a pulsed jet that may explain the stationary source, as suggested by Bally et al. (2003). Among these, the X-rays produced by the central protostar may be reflected into our line of sight by a scattering layer located about 100−200 AU from the parent star (a mechanism similar to that observed in Seyfert 2 galaxies). Alternatively, near the location of jet collimation the dense medium or the magnetic field could act like a nozzle leading to quasi-stationary shocks emitting X-rays (see discussions in Bonito et al. 2007).
- **Previously detected sources show detectable proper motion.** The new observations may show that the X-ray sources are located in different positions with respect to previous observations. This may happen because of the proper motion of the knots (not detectable on time-scales of 4 years but measurable on a time-scales of 10 years) or because new knots have emerged, while those observed in 2001 and 2005 have faded, giving the impression of a motion of the sources. Both cases are predicted by our model.
- **New sources appeared.** Our model predicts that the brightness and the morphology of the X-ray source associated with the pulsed jet can strongly change over time-scales on the order of 10 years. We expect therefore that new observations may show a very different morphology of HH 154, with new emerging knots and X-ray features (e.g. stationary shocks) catching the previously existing ones. This is probably the most frequent configuration predicted by the model.
- **Previously detected sources disappeared.** Since the last observation of HH 154 with Chandra has been performed in 2005, the time-lapse between this and a new observation will be at least 5 years, with a total time baseline since the first observation in 2001 of about 10 years. Over this time-scale, the sources can both disappear, which is also predicted by our model. Indeed, if the X-ray source is not powered by new energetic blobs, its X-ray luminosity drops with a characteristic time-scale of a few years.

5. Conclusions

We investigated the X-ray emission expected to arise from a randomly pulsed jet with the aim to explain the nature of X-ray emission detected in protostellar jets. We also explored the observable X-ray features predicted to form as a consequence of the collisions between blobs and knots within the jet by exploring the parameter space given by the ejection rate, initial jet Mach number, and initial density contrast between the ambient medium and the jet. Our findings lead to the following conclusions:

- In all the cases, the interactions of the ejected plasma blobs with the surrounding medium produce X-ray-emitting features. The main components contributing to the X-ray emission are irregular chains of knots, isolated high speed knots, steady knots, reverse shocks, and oblique shocks.
- Light jets produce significant X-ray emission consistent with the levels observed, whereas heavy jets are characterized by very faint or no X-ray emission and emit mostly in the optical band.
- For light jets (leading to detectable X-ray emission) the X-ray luminosity is mainly determined by the ejection rate of plasma blobs, rather than by the jet Mach number: higher ejection rates are related to more energetic objects, thus leading to higher X-ray luminosities.
- Our model predicts an X-ray luminosity and best-fit temperature that nicely agree with most of observed X-ray-emitting jets. In particular the HH 154 jet is well described as a pulsed jet with an ejection rate corresponding to $\Delta t = 2$ yr. Our model represents the first attempt to describe all the X-ray-emitting jets detected so far.
- We found that most of the X-ray emission is located at the base of the optical jet where the plasma blob collisions are the most energetic and where therefore the probability to detect X-ray emission is the highest. This result is consistent with the evidence that almost all LM objects show emission localized preferentially at the base of the jet.

In conclusion, our model explains why only a small fraction of HH jets has been detected in X-rays. Indeed, detectable X-ray emission may arise only under favorite conditions, namely high ejection rates of plasma blobs and high density contrast between the perturbed ambient medium and the ejected blob.

We stress that erroneous interpretations of observations can easily be drawn if the X-ray sources (reverse shocks, stationary knots, etc.) are not monitored frequently, since they show fast variability over time-scales of a few years. In this respect, numerical models can provide strong diagnostic tools to

interpret observations. To this end, we here provided model predictions about the morphology and characteristics of the X-ray source associated with HH 154 that may be revealed in future observations.

Acknowledgements. We thank Joel Kastner and Ettore Flaccomio for providing us the spectral parameters of the COUP source HH 540. R.B., S.O., M.M, and G.P. acknowledge support by the Marie Curie Fellowship Contract No. MTKD-CT-2005-029768. The software used in this work was in part developed by the DOE-supported ASC/Alliances Center for Astrophysical Thermonuclear Flashes at the University of Chicago, using modules for thermal conduction and optically thin radiation constructed at the Osservatorio Astronomico di Palermo. The calculations were performed on the cluster at the SCAN (Sistema di Calcolo per l'Astrofisica Numerica) facility of the INAF – Osservatorio Astronomico di Palermo and at CINECA (Bologna, Italy). This work was supported in part by Agenzia Spaziale Italiana under contract No. ASI-INAF I/088/06/0.

References

Bally, J., Feigelson, E., & Reipurth, B. 2003, ApJ, 584, 843
Bonito, R., Orlando, S., Peres, G., Favata, F., & Rosner, R. 2004, A&A, 424, L1
Bonito, R., Orlando, S., Peres, G., Favata, F., & Rosner, R. 2007, A&A, 462, 645
Bonito, R., Fridlund, C. V. M., Favata, F., et al. 2008, A&A, 484, 389
Bonito, R., Orlando, S., Peres, G., et al. 2010, A&A, 511, A42
Cowie, L. L., & McKee, C. F. 1977, ApJ, 211, 135
Favata, F., Bonito, R., Micela, G., et al. 2006, A&A, 450, L17
Fryxell, B., Olson, K., Ricker, P., et al. 2000, ApJS, 131, 273
Grosso, N., Feigelson, E. D., Getman, K. V., et al. 2006, A&A, 448, L29
Güdel, M., Skinner, S. L., Briggs, K. R., et al. 2005, ApJ, 626, L53
Güdel, M., Skinner, S. L., Audard, M., Briggs, K. R., & Cabrit, S. 2008, A&A, 478, 797
Kastner, J. H., Franz, G., Grosso, N., et al. 2005, ApJS, 160, 511
Linsky, J. L., Gagné, M., Mytyk, A., McCaughrean, M., & Andersen, M. 2007, ApJ, 654, 347
Pravdo, S. H., & Marshall, F. E. 1981, ApJ, 248, 591
Pravdo, S. H., Feigelson, E. D., Garmire, G., et al. 2001, Nature, 413, 708
Pravdo, S. H., Tsuboi, Y., & Maeda, Y. 2004, ApJ, 605, 259
Pravdo, S. H., Tsuboi, Y., Uzawa, A., & Ezoe, Y. 2009, ApJ, 704, 1495
Raga, A. C., de Colle, F., Kajdič, P., Esquivel, A., & Cantó, J. 2007, A&A, 465, 879
Spitzer, L. 1962, Physics of Fully Ionized Gases (New York: Interscience)
Stelzer, B., Hubrig, S., Orlando, S., et al. 2009, A&A, 499, 529
Tsuboi, Y., Koyama, K., Hamaguchi, K., et al. 2001, ApJ, 554, 734
Tsujimoto, M., Koyama, K., Kobayashi, N., et al. 2004, PASJ, 56, 341